

Article

Prediction of Superconductivity in Clathrate Er Hydrides under High Pressure

Xiao Z. Yan ¹, Zhao L. Zhang ¹, Yang M. Chen ^{1,*} and Fang G. Kuang ²

¹ School of Science, Jiangxi University of Science and Technology, Ganzhou 341000, China; yanxiaozen@jxust.edu.cn (X.Z.Y.)

² School of Physics and Electronic Information, Gannan Normal University, Ganzhou 341000, China

* Correspondence: chenyangmei@jxust.edu.cn

Abstract: In this paper, we perform unbiased structure searches combined with first-principles calculations to predict the stable structures and possible superconductivity of ErH_n ($n = 4\sim 6$) under pressures of 50–300 GPa. Two novel compounds, ErH_4 and ErH_6 , are identified as thermodynamically and dynamically stable above 50 GPa; ErH_4 and ErH_6 can stabilize in clathrate structures with the $I4/mmm$ and $Im\bar{3}m$ space groups, respectively. An analysis of the electronic density of states (DOS) suggests the metallic nature of the two phases. Then, the superconducting critical temperature (T_c) is estimated using the Allen–Dynes modified McMillan equation; the results are 130.9–181.2 K for $Im\bar{3}m\text{-ErH}_6$ at 100–300 GPa, and 74.4–79.8 K for $I4/mmm\text{-ErH}_4$ at 150–300 GPa. The resultant high T_c superconductivity in this system can be traced back to the combination of high density of states at the Fermi level and strong electron–phonon interactions.

Keywords: superconductivity; clathrate structure; high pressure; metal hydrides

1. Introduction

Searching for high-temperature superconductors is a hot topic in condensed-matter physics and materials science [1–6]. Metallic hydrogen has been predicted to be a superconductor with high transition temperatures [1]. However, it is technically difficult to attain metallic states of hydrogen through static compression experiments. Searching for high- T_c superconductors has, in turn, transformed to some other systems such as hydrogen-dominant compounds [2]. According to Ashcroft’s prediction [2], hydrogen-rich hydrides can be metallized at much lower pressures compared to elemental hydrogen due to chemical “pre-compression” effects, and therefore, may be potential superconductors with high T_c . This finding promoted the subsequent upsurge in the study of hydrides and which has eventually led to the discovery of a plethora of superconducting hydrides.

Alkali metals (AM = Li, Na, K, Rb, and Cs) comprise one of the most reactive groups of elements that can react with hydrogen at atmospheric conditions, forming alkali hydrides in the rock–salt (B1) structure with AMH stoichiometry. These hydrides are classic ionic compounds with large energy band gaps of 4–6 eV [7]. Although theoretical calculations have suggested that pressure-induced metallization takes place at ~300 GP, these systems are not good candidates for high temperature superconductivity even under high pressures, since they are unlikely to have high density of states (DOS) values at the Fermi level (E_F). However, by compressing mixtures of AMH and H_2 , alkali metal subhydrides (AMH_x , $x > 1$) have been predicted to become stable (or metastable) under high pressures [8,9]. Among these alkali metal subhydrides, LiH_6 (with $R3m$ symmetry), LiH_8 (with $I422$ symmetry), and KH_6 (with $C2/c$ symmetry) are superconductors with T_c values of 38–82 K at 150–300 GPa, 31–37 K at 100–200 GPa, and 46–70 K at 230–300 GPa, respectively [10,11]. These calculations suggest that alkali metal hydrides with high DOS values at E_F are more likely to have high T_c superconductivity.



Citation: Yan, X.Z.; Zhang, Z.L.; Chen, Y.M.; Kuang, F.G. Prediction of Superconductivity in Clathrate Er Hydrides under High Pressure. *Crystals* **2023**, *13*, 792. <https://doi.org/10.3390/cryst13050792>

Academic Editor: Russell Hemley

Received: 26 March 2023

Revised: 29 April 2023

Accepted: 3 May 2023

Published: 9 May 2023



Copyright: © 2023 by the authors. Licensee MDPI, Basel, Switzerland. This article is an open access article distributed under the terms and conditions of the Creative Commons Attribution (CC BY) license (<https://creativecommons.org/licenses/by/4.0/>).

Meanwhile, alkaline earth metal hydrides have also been studied using DFT calculations [12,13]. Due to the lower DOS values at E_F , BeH_2 and MgH_2 have been predicted to have smaller T_c values of 32–44 K at 250 GPa [12] and 16–23 K at 180 GPa [13], respectively. However, by increasing the H content, CaH_6 [14] and MgH_6 [15], calculations have shown they can be stable above 150 GPa. Interestingly, both of the hydrides crystallize in sodalite-like clathrate structures (in a space group of $Im\bar{3}m$) with hydrogenic frameworks. The estimated T_c values exhibit highs of 235 K for CaH_6 at 150 [14] GPa and 263–271 K at 300–400 GPa for MgH_6 [15]. The ultrahigh T_c values in these systems arise from a substantial DOS value at E_F , contributed primarily from hydrogen atoms which comprise the hydrogenic lattices. Therefore, it has been proposed that systems with extended hydrogenic lattices are more likely to become superconductors at higher temperatures. A recent experimental investigation successfully synthesized CaH_6 and verified the superconductivity with a measured T_c of 215 K at 172 GPa [16].

Encouraged by the seminal finding in CaH_6 , extensive theoretical and experimental investigations have been carried out to search for hydrides with extended hydrogenic lattices. The hydrides with d -block elements are typical examples. A large number of scandium, yttrium, and lanthanum hydrides have been predicted to be stable under high pressures, and some of them have had high calculated T_c values. For example, ScH_6 was predicted to stabilize in a structure isotypic with CaH_6 at pressures above 265 GPa [17]. ScH_x ($x = 7\text{--}10$ and 12) was predicted to be synthesized by compressing mixtures of ScH_3 and H_2 above 150 GPa, forming the $Cmcm$, $Immm$, $P6_3/mmc$, $Cmcm$, and $C2/c$ structures, respectively [18,19]. The calculated T_c values of these systems were reported to be 120–169 K at pressures above 250 GPa [19].

Similar to CaH_6 , theoretical calculations have shown that H clathrate structures could also be formed in rare earth (RE) hydrides such as REH_6 , REH_9 , and REH_{10} , where RE = Y, La, Ce, and Pr [4]. These compounds are peculiar, since the H atoms in their structures are weakly covalently bonded with each other, forming unusual H cages with stoichiometries of H_{24} , H_{29} , and H_{32} . The estimated T_c values of these systems are striking [3,4,20]. YH_{10} and LaH_{10} (both within the $Fm\bar{3}m$ symmetry) have been predicted to be potential room temperature superconductors with maximum T_c values of 303–326 K at 250–400 GPa and 274–286 K at 210–250 GPa, respectively [3,4]. Remarkably, some of these materials, consistent with the theoretically predicted structures, have been successfully synthesized in recent experiments [21]. For example, YH_6 and YH_9 were measured to have T_c values of 220 K at 166 GPa [22] and 243 K at 201 GPa [23], respectively. LaH_{10} was experimentally synthesized to exhibit a T_c value of 250 K at 170 GPa [6]. Synthesized LaH_9 and CeH_9 alloys exhibited T_c values of 148–178 K in the pressure range of 97–172 GPa [24]. At much lower pressures, the T_c values of CeH_9 (with the $Fm\bar{3}m$ structure) and CeH_{10} (with the $P6_3/mmc$ structure) were measured to be 57 K at 88 GPa and 115 K at 95 GPa [25,26], respectively. However, the theoretically predicted YH_{10} and its highest $T_c > 300$ K has not yet been observed in experiments [23].

As the neighbor elements of Sc and Y, the high-pressure structures and superconductivities of titanium (Ti), zirconium (Zr), and hafnium (Hf) hydrides have also been studied. However, these systems have not exhibited good superconducting properties. The ZrH phase with a $Cmcm$ structure and HfH_2 phase with a $P2_1/m$ structure are the only two phases that have been identified to exhibit significant electron–phonon coupling (EPC). The maximum T_c values have been estimated to be 10.6 K for ZrH at 120 GPa [27] and 12.8 K for HfH_2 at 260 GPa [28]. In the group V metal hydrides, only the $I4/mmm$ phase of NbH_4 has been calculated to have a T_c of 47 K at 300 GPa [29]. The relatively higher T_c in this phase can be traced back to the larger EPC parameter and average logarithmic frequency.

In addition to the above hydrides with metal elements, interesting superconductivity properties have also been discovered in hydrides with non-metal elements. The sulfur hydride is one of the most favorable examples, which has been studied extensively in experiments and calculations.

Theoretical calculations have indicated that H₂S is thermodynamically and dynamically stable, up to 200 GPa [30]. The calculated T_c was 80 K in the *Cmca*-H₂S [31]. H₃S has been predicted to stabilize in the *R3m* and *Im $\bar{3}m$* phases at pressures of 111 and 180 GPa, respectively [31]. The two structures both have a particularly high EPC, which leads to high T_c values of 155~166 K at 130 GPa and 191~204 K at 200 GPa [31]. Recent experimental investigations have confirmed the ultrahigh T_c superconductivity in the *Im $\bar{3}m$* phase H₃S under high pressure [31]. In addition, high T_c superconductivity has also been predicted in other sulfides. For example, in the H-S-P system (H₃S_{0.925}P_{0.075}), the maximum T_c was theoretically estimated to be 280 K at 250 GPa [32]. In the C-S-H system, a T_c of 260 K at 133 GPa was reported in a recent experiment with a modulated AC susceptibility technique adapted for a diamond anvil cell [33]. This experiment revealed a *Pnma* structure of the material which was responsible for the near room-temperature superconductivity of carbonaceous sulfur hydride at 107–133 GPa [33].

Following the discovery of striking superconductivity in sulfur hydrides, the potential superconductivities of hydrides with isoelectronic selenium (Se) and tellurium (Te) have also been investigated under high pressures. H₃Se was predicted to stabilize in the *Im $\bar{3}m$* phase above 200 GPa [34], which is isostructural to H₃S. Due to a smaller EPC parameter compared to H₃S, DFT calculations yielded a lower T_c value of 130 K for H₃Se at 200 GPa [34]. In the Te-H system, the structures and stoichiometries were somehow different from those of sulfur and selenium. DFT calculations showed that *P6₃/mmm*-H₄Te, *C2/m*-H₅Te₂, and *P6₃/mmc*-H₇Te were the most stable phases at 200 GPa [35]. The stoichiometry of H₃Te stabilized in a *C2/m* structure above 300 GPa. The largest T_c in Te-H systems was obtained in the H₄Te phase, of which the calculated value was 104 K at 170 GPa [35]. Furthermore, superconductivity has also been reported in some other hydrides. For example, an experimental study indicated that PH₃ exhibited superconductivity with a maximum measured T_c of 100 K at 207 GPa [36]. DFT calculations estimated a T_c of 150 K for AsH₈ at 350 GPa [37].

As demonstrated by the above investigations, metal hydrides with clathrate structures are a special class of H-rich compounds that may achieve high T_c superconductivity approaching or exceeding room temperature. The reason why they have such a high T_c can be traced back to the combination of a high density of states near E_F and strong electron–phonon interactions.

The rare earth element erbium (Er), with partially filled *f* orbitals, is one of the most reactive metal elements, which results in unique electronic and bonding properties. Under ambient conditions, erbium reacts with hydrogen, consecutively forming metallic ErH₂ with a CaF₂-type structure and insulating ErH₃ with a HoD₃-type structure [38]. Recent DFT calculations have demonstrated that ErH₂ could be a superconductor with a T_c of ~80 K at 14.5 GPa [39]. If sufficient pressure is applied to ErH₃, it can also be forced to be transformed into metallic states. However, no superconductivity has yet been observed for ErH₃ in previous theoretical and experimental studies at pressures up to 140 GPa [40–42]. In this paper, we perform systematic structure searches by increasing the H concentration in Er-H systems, with the aim of finding clathrate Er hydrides. Encouragingly, we do predict two novel stable clathrate Er hydrides with the stoichiometries of ErH₄ and ErH₆ in the pressure range of 50~300 GPa. It is found that both of the two clathrate hydrides can achieve high- T_c superconductivity.

2. Methods and Computational Details

The searching simulations of crystal structure with 1~4 formula units in the models of ErH_{*n*} (*n* = 4~6) were performed using the swarm-intelligence-based CALYPSO method and software [43,44], which has been successfully applied to predict the structures of many systems [45–48]. The structure optimizations and electronic property calculations were performed following the plane-wave basis projector-augmented-wave (PAW) method [49] in the framework of density functional theory as implemented in the Vienna ab initio simulation package (VASP) code [50]. In these calculations, the generalized gradient approxima-

tion in the Perdew–Burke–Ernzerhof [51] form is applied for the exchange–correlation functionals. The configurations of $5s^25p^66s^24f^{12}$ and $1s^1$ of Er and H, respectively, are treated as valence electrons for the PAW pseudopotentials. The cutoff energy is set to 650 eV, and the Monkhorst–Pack grid with a maximum spacing of 0.03 \AA^{-1} is individually adjusted in reciprocal space to the size of each computational cell. The density functional perturbation theory, as implemented in the Quantum ESPRESSO (QE) package [52], is used to examine the dynamical stability and to calculate the electron–phonon coupling (EPC) parameters of these compounds. The Troullier–Martins norm-conserving scheme is used to generate the pseudopotentials for H and Er, wherein the Er $4f$ electrons are treated as valence electrons. The Brillouin zone is sampled using a $4 \times 4 \times 4$ q-point grid in the calculations of the EPC parameters. A denser $24 \times 24 \times 24$ k-point mesh is used to accurately calculate the electron–phonon interaction matrix. The kinetic energy cutoffs are set to 70 Ry for the plane wave functions and 600 Ry for the charge density. The formation enthalpies (ΔH) of ErH_n are calculated by using: $\Delta H(\text{ErH}_n) = H(\text{ErH}_n) - H(\text{ErH}_3) - (0.5n - 1.5)H(\text{H}_2)$, where H is the enthalpy of the most stable structure of certain compositions at the given pressure. For ErH_3 , the $Fm\bar{3}m$ and $P6_3/mmc$ structures are considered [39], and for elemental H_2 , the $P6_3/m$, $C2/c$, and $Cmca$ -12 phases are used [53].

3. Results and Discussion

3.1. Crystal Structures and Stabilities

As mentioned in the Introduction, hydrides with high T_c benefit from the clathrate structures. To explore the superconductivity of the Er–H system, first, we search stable structures for ErH_n ($n = 4\sim 6$) at 50–300 GPa. The formation enthalpies (with respect to decomposition into ErH_3 and H_2) versus composition for the energy favorable structures of each compound are displayed in Figure 1, from which the thermodynamical stability can be obtained. The results show that no compounds are stable at 50 GPa, since all of the formation enthalpies are positive. When the pressure increases to 100 GPa, the formation enthalpies become negative. Meanwhile, ErH_4 and ErH_6 , which locate on the convex hull, become stable. As pressure further increases up to 200 and 300 GPa, ErH_4 and ErH_6 maintain their stabilities.

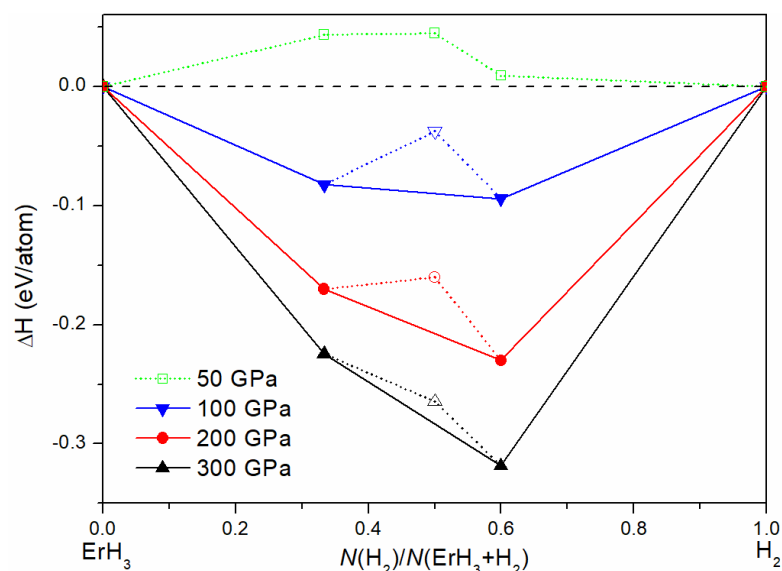


Figure 1. Enthalpies of ErH_n formation ($n = 4\sim 6$) at 50–300 GPa. The solid symbols connected by solid lines on the convex hull denote the stable phases against any type of decomposition. The open symbols located above the convex hull represent unstable or metastable phases. The colorful dotted and black dashed lines are for the eye-guide only.

Our structure searches show that both ErH_4 and ErH_6 crystallize in clathrate structures under high pressure. The pressure dependence of the enthalpy difference for the energy low-lying structures are plotted in Figure 2. In the case of ErH_6 , the clathrate structure stabilizes above 88 GPa and adopts an $Im\bar{3}m$ symmetry which is similar to that of XH_6 ($X = \text{Tb}, \text{Ca}, \text{Mg}, \text{Y}, \text{and Sc}$) [12,54]. As shown in Figure 3a, the $Im\bar{3}m$ - ErH_6 forms an H_{24} cage structure with the Er atoms locating at the cage center. The H_{24} cage consists of six squares and eight hexagons, and the H-H bond lengths in the both the squares and the hexagons are 1.17, 1.19, 1.21, 1.25, and 1.29 Å at 100, 150, 200, 250, and 300 GPa, respectively. These bond values are smaller than those in TbH_6 and CaH_6 , and larger than those in ScH_6 and MgH_6 at the same conditions [12,54]. The nearest H-Er distances are 2.04 Å and 1.85 Å at 100, 300 GPa, respectively. The crystal structure parameters of $Im\bar{3}m$ - ErH_6 and the other predicted stable phases are presented in Table 1.

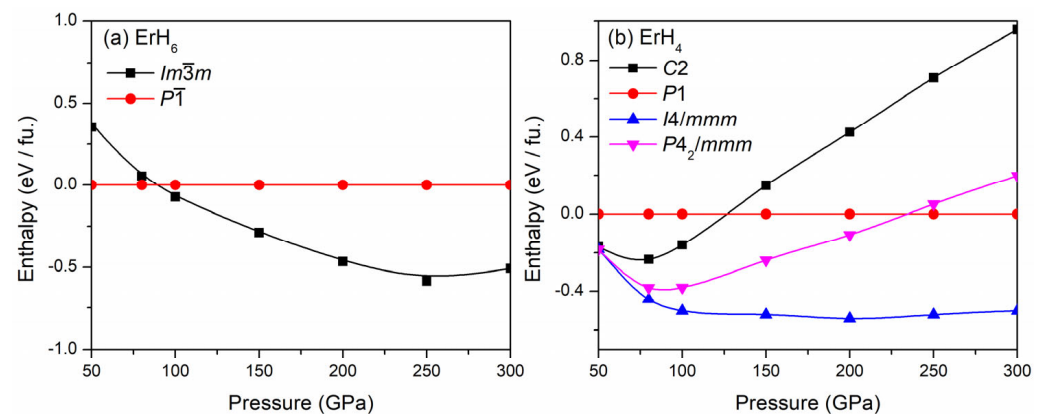


Figure 2. Pressure dependence of the enthalpy difference for the energy low-lying structures of: (a) ErH_6 ; (b) ErH_4 .

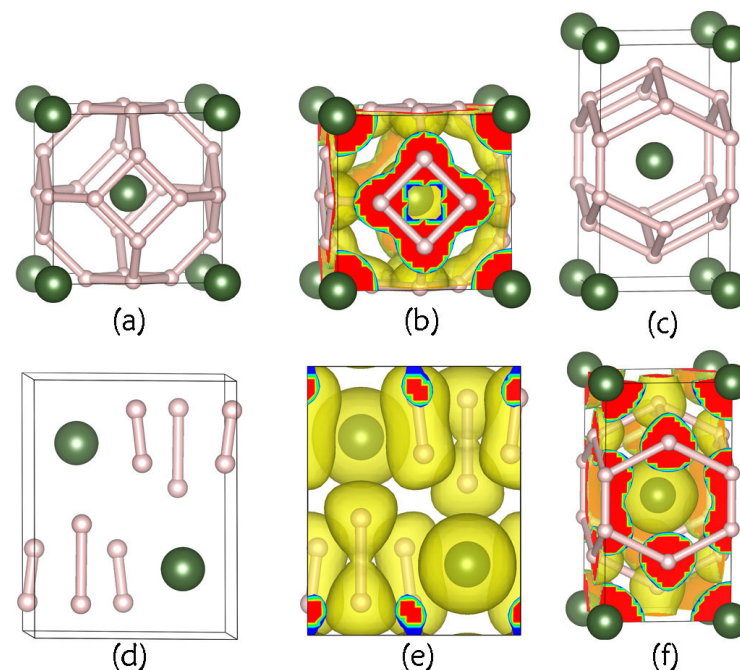


Figure 3. Crystal structures and bonding properties: (a) Structure of $Im\bar{3}m$ - ErH_6 ; (b) ELF of $Im\bar{3}m$ - ErH_6 at 100 GPa; (c) structure of $I4/mmm$ - ErH_4 ; (d) structure of $P\bar{1}$ - ErH_6 ; (e) ELF of $P\bar{1}$ - ErH_6 at 80 GPa; (f) ELF of $I4/mmm$ - ErH_4 at 100 GPa. The isosurface value of ELF is set to 0.5. Small and large spheres denote H and Er atoms, respectively.

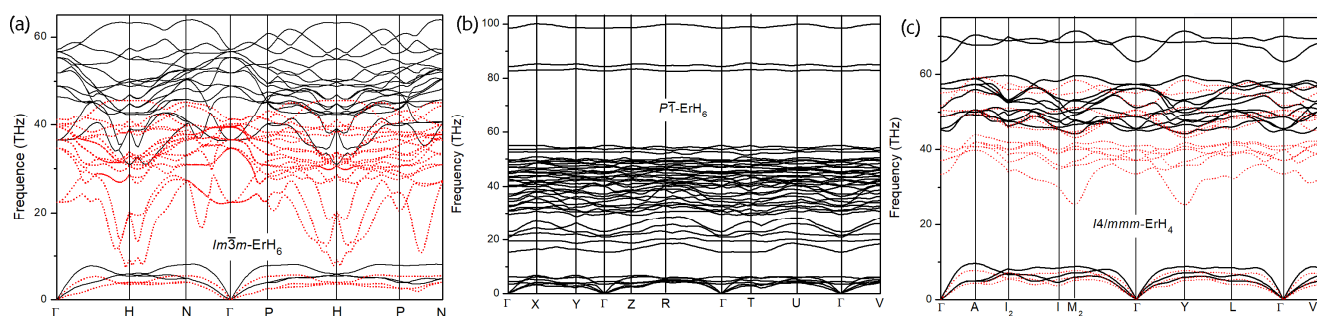
Table 1. Crystal lattice parameters of the predicted stable ErH_n phases under high pressures.

Phase	Pressure (GPa)	Lattice Parameters	Coordinates
$Im\bar{3}m\text{-ErH}_6$	100	$a = 3.16 \text{ \AA}$ $\alpha = 109.47$	H1 0.25000 0.50000 -0.25000
		$b = 3.16 \text{ \AA}$ $\beta = 109.47$	Er1 0.00000 0.00000 0.00000
$P\bar{1}\text{-ErH}_6$	80	$a = 3.15 \text{ \AA}$ $\alpha = 89.99$	H1 0.82939 0.51335 0.88270
		$b = 3.67 \text{ \AA}$ $\beta = 100.40$	H2 0.78475 0.54530 0.67573
		$c = 4.71 \text{ \AA}$ $\gamma = 89.99$	H3 0.36777 0.74998 0.87671
			H5 0.72069 0.24999 0.43394
			H6 0.82940 0.98659 0.88268
			H7 0.78476 0.95469 0.67571
$I4/mmm\text{-ErH}_4$	100	$a = 3.31 \text{ \AA}$ $\alpha = 129.59$	H1 1.38370 1.38370 1.00000
		$b = 3.31 \text{ \AA}$ $\beta = 129.59$	H2 0.75000 1.25000 0.50000
		$c = 3.31 \text{ \AA}$ $\gamma = 74.05$	Er1 0.00000 0.00000 0.00000

As shown in Figure 3b, the calculated electron localization function (ELF) [55] reveals weakly covalent bonding of H-H in the H_{24} cage. For example, the value of ELF is 0.59 at 100 GPa. It is worth noting that systems with weak covalent bonds are expected to reach high T_c superconductivity. From this point of view, it is necessary to investigate the superconductivity of $Im\bar{3}m\text{-ErH}_6$.

As revealed in Figure 2, the $Im\bar{3}m$ phase of ErH_6 is stable under pressures of 88~300 GPa. When the pressure decreases to below 88 GPa, it transforms to the $P\bar{1}$ phase. The H atoms in this phase form two types of H_2 units, as displayed in Figure 3d. The H-H bond lengths of the H_2 units are 0.97 and 1.44 Å at 80 GPa, respectively. The corresponding ELF (Figure 3e) values are 0.96 and 0.55, respectively, indicating different strengths of covalent bonding.

The phonon dispersions of ErH_6 at different pressures are plotted in Figure 4. It is shown that there is no imaginary frequency in the phonon spectra of $Im\bar{3}m\text{-ErH}_6$ at 100 and 300 GPa, indicating that they are dynamically stable (Figure 4a). A prominent feature of the $Im\bar{3}m$ phase is the drastic softening of the low-lying optical mode around the H point and along the $N\text{-}\Gamma$ and $P\text{-}N$ directions when the pressure decreases from 300 to 100 GPa. At 86 GPa, strong phonon softening leads to the emergence of imaginary frequencies at the H point and along the $P\text{-}N$ direction, which is responsible for the structural phase transition from $Im\bar{3}m$ to $P\bar{1}$. The dynamical stability of $P\bar{1}\text{-ErH}_6$ is also revealed by the phonon spectra, as presented in Figure 4b.

**Figure 4.** Phonon dispersions of: (a) $Im\bar{3}m\text{-ErH}_6$ at 100 GPa (dotted line) and 300 GPa (solid line); (b) $P\bar{1}\text{-ErH}_6$ at 80 GPa; (c) $I4/mmm\text{-ErH}_4$ at 150 GPa (dotted line) and 300 GPa (solid line), respectively.

For ErH_4 , the clathrate structure is the only thermodynamically stable phase above 50 GPa. This phase shares the same crystal structure of $I4/mmm$ with TbH_4 [45]. As presented in Figure 3c, the H atoms in this phase form a cage-like structure of H_{18} , containing eight quadrilaterals and four hexagons. There are two types of H-H bonds in $I4/mmm\text{-ErH}_4$, and the bond lengths are 1.36 and 1.39 Å at 300 GPa, and 1.58 and 1.23 Å at 100 GPa,

respectively. The corresponding values of ELF (Figure 3f) are 0.52 and 0.45 at 300 GPa, and 0.41 and 0.73 at 100 GPa, respectively. This result indicates that the H-H covalent bonds present opposite responses of compression, i.e., the former is strengthened by pressure and the latter is weakened. The dynamical stability of this phase can also be demonstrated by the phonon dispersions presented in Figure 4c.

3.2. Electronic Characteristics and Superconductivity

To analyze the electronic properties of ErH_n , we calculate the electronic density of states (DOS). Our results indicate that all the stable Er-H phases predicted here exhibit metallic nature in the corresponding stable pressure range. It is worth noting that even crystallized in different structures, the DOS distributions of $Im\bar{3}m\text{-ErH}_6$, $P\bar{1}\text{-ErH}_6$, and $I4/mmm\text{-ErH}_4$ bear strong resemblance to each other. As shown in Figure 5, the projected DOS on different orbitals of Er and H atoms all cross at the Fermi level. The electronic states around the Fermi level are mainly contributed from Er-*f*, Er-*d*, and H-*s* orbitals, while the contribution of Er-*s* and Er-*p* are relatively scanty. Another overall feature of the DOS results is the broadening of Er-*f* electronic states, indicating that the 4*f* electrons are delocalized and the electronic correlation effect is weakened by pressure.

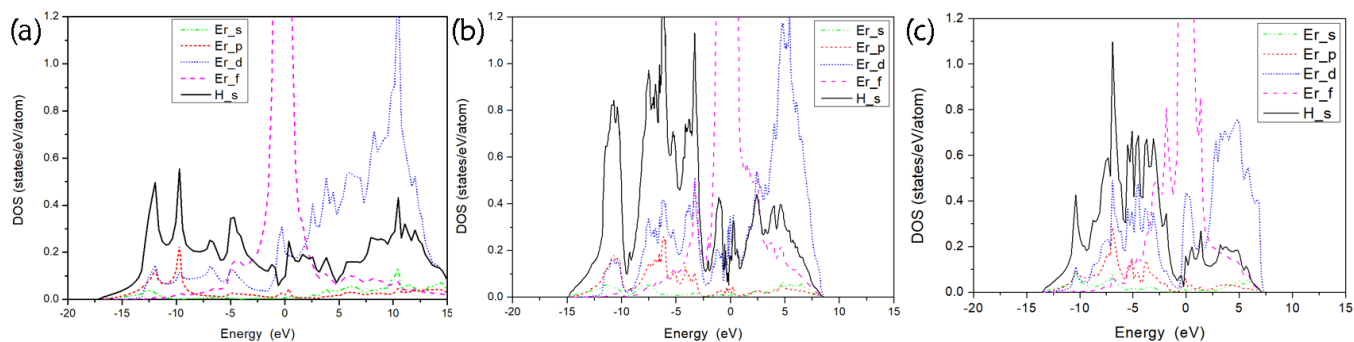


Figure 5. Projected density of states (DOS) of: (a) $Im\bar{3}m\text{-ErH}_6$ at 100 GPa; (b) $P\bar{1}\text{-ErH}_6$ at 80 GPa; (c) $I4/mmm\text{-ErH}_4$ at 100 GPa. The Fermi energy is set at 0 eV.

To assess the superconductivity of the Er-H systems, the Eliashberg electron–phonon spectral function [$\alpha^2F(\omega)$], the EPC parameter (λ), and the logarithmic average of phonon frequency (ω_{\log}) are then calculated. As shown in Figure 6, for $Im\bar{3}m\text{-ErH}_6$, the EPC parameters are calculated to be 3.89 and 1.60 at 100 and 300 GPa, respectively. The corresponding values of ω_{\log} are 857.4 K and 1427.8 K, respectively. The vibrations of H atoms which dominate the medium- and high-frequency region in the phonon DOS contribute 84% and 80% to the total EPC at 100 and 300 GPa, respectively. The strong EPC of this phase at low pressure is attributed to the strong phonon softening (Figure 4). For $P\bar{1}\text{-ErH}_6$, the absence of H cage structure leads to a much weaker EPC of $\lambda = 0.48$ at 80 GPa. However, the ω_{\log} still has a considerable value of 944.8 K at this pressure, attributing to the high content of H. Different from the $Im\bar{3}m$ phase, the contribution of H-atom vibrations located in the medium frequency (15~46 THz) contribute mainly (75%) to the total EPC in the $P\bar{1}\text{-ErH}_6$. The contribution of high-frequency vibrations is only 3%.

In the case of $I4/mmm\text{-ErH}_4$, the electron–phonon interaction is also considerable. The calculated values of λ are 0.96 and 0.85 at 150 and 300 GPa, respectively, and the corresponding ω_{\log} values are 1231.7 and 1379.9 K, respectively. Similar to $Im\bar{3}m\text{-ErH}_6$, the vibrations of H atoms both in the medium- and high-frequency region contribute dominantly to the total EPC.

Based on the above data combined with a typical Coulomb pseudopotential value of $\mu^* = 0.1$, the superconducting critical temperature (T_c) values can be estimated in terms of the Allen–Dynes modified McMillan equation [56]. The obtained T_c of $Im\bar{3}m\text{-ErH}_6$ reaches high values of 130.9 K and 181.2 K at 100 GPa and 300 GPa, respectively. However, the $P\bar{1}\text{-ErH}_6$ has a much lower T_c of 9.3 K at 80 GPa, because of the absence of H cage structure.

For $I4/mmm$ -ErH₄, the EPC is relatively weak and the resultant T_c values are 74.4 K and 79.8 K at 150 GPa and 300 GPa, respectively. This result indicates that the cage structure of H atoms obviously leads to higher superconducting critical temperatures, which is consistent with the perspectives of Zurek et al [57].

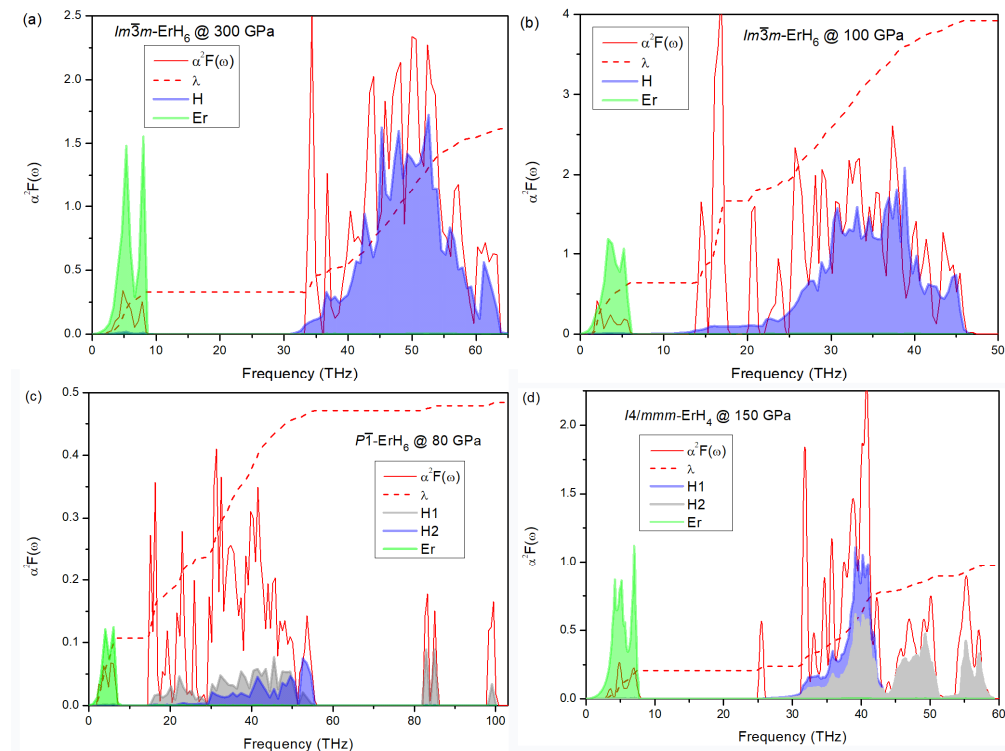


Figure 6. Eliashberg electron–phonon spectral function $\alpha^2F(\omega)$ (solid line), the integral EPC parameter λ (dashed line) as a function of frequency, and the corresponding phonon DOS (dash area) of (a) $Im\bar{3}m$ -ErH₆ at 300 GPa; (b) $Im\bar{3}m$ -ErH₆ at 100 GPa; (c) $P\bar{1}$ -ErH₆ at 80 GPa; (d) $I4/mmm$ -ErH₄ at 150 GPa.

4. Conclusions

In summary, we have predicted two new Er hydrides with the stoichiometries of ErH₄ and ErH₆, using the CALYPSO crystal structure prediction method combined with first-principles calculations. ErH₄ was predicted to crystallize in a clathrate structure in the whole pressure range considered here. This phase has a space group of $I4/mmm$, wherein the H atoms bond to each other and form H₁₈ cages. ErH₆ was also predicted to stabilize in a clathrate structure with the space group of $Im\bar{3}m$ at pressures above 88 GPa. In this phase, the H atoms form a H₂₄ cage sublattice. As pressure decreases to below 88 GPa, the $Im\bar{3}m$ phase transforms to a low symmetrical phase with a space group of $P\bar{1}$, attributed to the strong phonon softening. All of the predicted phases exhibit good metallic nature at their stable pressure ranges. The estimated maximum value of T_c in the Er-H system is obtained in the $Im\bar{3}m$ phase of ErH₆, which reaches a high value of 181.2 K at 300 GPa. Our results enrich the family of rare earth hydrides and may help with the further discovery of room temperature superconductors in metal hydrides.

Author Contributions: Conceptualization, X.Z.Y. and Y.M.C.; investigation, X.Z.Y., Z.L.Z., Y.M.C. and F.G.K.; data curation, X.Z.Y. and Z.L.Z.; writing—original draft preparation, X.Z.Y.; writing—review and editing, X.Z.Y. All authors have read and agreed to the published version of the manuscript.

Funding: This work is supported by the National Natural Science Foundation of China under grant nos. 11704163, 11804131, and 11964001; the Educational Commission of Jiangxi Province of China under grant no. GJJ200862; the Natural Science Foundation of Jiangxi Province of China under grant no. 20181BAB211007.

Data Availability Statement: Not applicable.

Conflicts of Interest: The authors declare no conflict of interest.

References

1. Ashcroft, N.W. Metallic Hydrogen: A High-Temperature Superconductor? *Phys. Rev. Lett.* **1968**, *21*, 1748–1749. [[CrossRef](#)]
2. Ashcroft, N.W. Hydrogen Dominant Metallic Alloys: High Temperature Superconductors? *Phys. Rev. Lett.* **2004**, *92*, 187002. [[CrossRef](#)] [[PubMed](#)]
3. Liu, H.; Naumov, I.I.; Hoffmann, R.; Ashcroft, N.W.; Hemley, R.J. Potential High-Tc Superconducting Lanthanum and Yttrium Hydrides at High Pressure. *Proc. Natl. Acad. Sci. USA* **2017**, *114*, 6990–6995. [[CrossRef](#)]
4. Peng, F.; Sun, Y.; Pickard, C.J.; Needs, R.J.; Wu, Q.; Ma, Y. Hydrogen Clathrate Structures in Rare Earth Hydrides at High Pressures: Possible Route to Room-Temperature Superconductivity. *Phys. Rev. Lett.* **2017**, *119*, 107001. [[CrossRef](#)] [[PubMed](#)]
5. Somayazulu, M.; Ahart, M.; Mishra, A.K.; Geballe, Z.M.; Baldini, M.; Meng, Y.; Struzhkin, V.V.; Hemley, R.J. Evidence for Superconductivity above 260 K in Lanthanum Superhydride at Megabar Pressures. *Phys. Rev. Lett.* **2019**, *122*, 027001. [[CrossRef](#)]
6. Drozdov, A.P.; Drozdov, A.P.; Kong, P.P.; Minkov, V.S.; Besedin, S.P.; Kuzovnikov, M.A.; Mozaffari, S.; Balicas, L.; Balakirev, F.F.; Graf, D.E.; et al. Superconductivity at 250 K in Lanthanum Hydride under High Pressures. *Nature* **2019**, *569*, 528–531. [[CrossRef](#)]
7. Van Setten, M.J.; Popa, V.A.; de Wijs, G.A.; Brocks, G. Electronic Structure and Optical Properties of Lightweight Metal Hydrides. *Phys. Rev. B* **2007**, *75*, 035204. [[CrossRef](#)]
8. Zurek, E.; Hoffmann, R.; Ashcroft, N.W.; Oganov, A.R.; Lyakhov, A.O. A Little Bit of Lithium Does a Lot for Hydrogen. *Proc. Natl. Acad. Sci. USA* **2009**, *106*, 17640–17643. [[CrossRef](#)]
9. Chen, Y.; Geng, H.Y.; Yan, X.; Sun, Y.; Wu, Q.; Chen, X. Prediction of Stable Ground-State Lithium Polyhydrides under High Pressures. *Inorg. Chem.* **2017**, *56*, 3867–3874. [[CrossRef](#)]
10. Xie, Y.; Li, Q.; Oganov, A.R.; Wang, H. Superconductivity of Lithium-Doped Hydrogen under High Pressure. *Acta Cryst.* **2014**, *70*, 104–111. [[CrossRef](#)]
11. Zhou, D.; Jin, X.; Meng, X.; Bao, G.; Ma, Y.; Liu, B.; Cui, T. Ab Initio Study Revealing a Layered Structure in Hydrogen-Rich KH₆ under High Pressure. *Phys. Rev. B* **2012**, *86*, 014118. [[CrossRef](#)]
12. Yu, S.; Zeng, Q.; Oganov, A.R.; Hu, C.; Frapper, G.; Zhang, L. Exploration of Stable Compounds, Crystal Structures, and Superconductivity in the Be-H System. *AIP Adv.* **2014**, *4*, 107118. [[CrossRef](#)]
13. Lonie, D.C.; Hooper, J.; Altintas, B.; Zurek, E. Metallization of Magnesium Polyhydrides under Pressure. *Phys. Rev. B* **2013**, *87*, 054107. [[CrossRef](#)]
14. Wang, H. Superconductive Sodalite-Like Clathrate Calcium Hydride at High Pressures. *Proc. Natl. Acad. Sci. USA* **2012**, *109*, 4. [[CrossRef](#)]
15. Feng, X.; Zhang, J.; Gao, G.; Liu, H.; Wang, H. Compressed Sodalite-Like MgH₆ as a Potential High-Temperature Superconductor. *RSC Adv.* **2015**, *5*, 59292–59296. [[CrossRef](#)]
16. Ma, L.; Wang, K.; Xie, Y.; Yang, X.; Wang, Y.; Zhou, M.; Liu, H.; Yu, X.; Zhao, Y.; Wang, H.; et al. High-Temperature Superconducting Phase in Clathrate Calcium Hydride CaH₆ up to 215 K at a Pressure of 172 Gpa. *Phys. Rev. Lett.* **2022**, *128*, 167001. [[CrossRef](#)]
17. Abe, K. Hydrogen-Rich Scandium Compounds at High Pressures. *Phys. Rev. B* **2017**, *96*, 144108. [[CrossRef](#)]
18. Qian, S.; Sheng, X.; Yan, X.; Chen, Y.; Song, B. Theoretical Study of Stability and Superconductivity of ScH_n (n = 4–8) at High Pressure. *Phys. Rev. B* **2017**, *96*, 094513. [[CrossRef](#)]
19. Ye, X.; Zarifi, N.; Zurek, E.; Hoffmann, R.; Ashcroft, N.W. High Hydrides of Scandium under Pressure: Potential Superconductors. *J. Phys. Chem. C* **2018**, *122*, 6298–6309. [[CrossRef](#)]
20. Heil, C.; Di Cataldo, S.; Bachelet, G.B.; Boeri, L. Superconductivity in Sodalite-Like Yttrium Hydride Clathrates. *Phys. Rev. B* **2019**, *99*, 220502. [[CrossRef](#)]
21. Geballe, Z.M.; Liu, H.; Mishra, A.K.; Ahart, M.; Somayazulu, M.; Meng, Y.; Baldini, M.; Hemley, R.J. Synthesis and Stability of Lanthanum Superhydrides. *Angew. Chem. Int. Edit.* **2018**, *57*, 688–692. [[CrossRef](#)] [[PubMed](#)]
22. Troyan, I.A.; Semenok, D.V.; Kvashnin, A.G.; Sadakov, A.V.; Sobolevskiy, O.A.; Pudalov, V.M.; Ivanova, A.G.; Prakapenka, V.B.; Greenberg, E.; Gavriliuk, A.G.; et al. Anomalous High-Temperature Superconductivity in YH₆. *Adv. Mater.* **2021**, *33*, 2006832. [[CrossRef](#)] [[PubMed](#)]
23. Kong, P.; Minkov, V.S.; Kuzovnikov, M.A.; Drozdov, A.P.; Besedin, S.P.; Mozaffari, S.; Balicas, L.; Balakirev, F.F.; Prakapenka, V.B.; Chariton, S. Superconductivity up to 243 K in the Yttrium-Hydrogen System under High Pressure. *Nat. Commun.* **2021**, *12*, 5075. [[CrossRef](#)]
24. Bi, J.; Nakamoto, Y.; Zhang, P.; Shimizu, K.; Zou, B.; Liu, H.; Zhou, M.; Liu, G.; Wang, H.; Ma, Y. Giant Enhancement of Superconducting Critical Temperature in Substitutional Alloy (La,Ce)H₉. *Nat. Commun.* **2022**, *13*, 5952. [[CrossRef](#)] [[PubMed](#)]
25. Chen, W.; Semenok, D.V.; Huang, X.; Shu, H.; Li, X.; Duan, D.; Cui, T.; Oganov, A.R. High-Temperature Superconducting Phases in Cerium Superhydride with a Tc up to 115 K Below a Pressure of 1 Megabar. *Phys. Rev. Lett.* **2021**, *127*, 117001. [[CrossRef](#)]
26. Salke, N.P.; Esfahani, M.M.D.; Zhang, Y.; Kruglov, I.A.; Zhou, J.; Wang, Y.; Greenberg, E.; Prakapenka, V.B.; Liu, J.; Oganov, A.R. Synthesis of Clathrate Cerium Superhydride CeH₉ at 80–100 GPa with Atomic Hydrogen Sublattice. *Nat. Commun.* **2019**, *10*, 4453. [[CrossRef](#)]

27. Li, X.-F.; Hu, Z.-Y.; Huang, B. Phase Diagram and Superconductivity of Compressed Zirconium Hydrides. *Phys. Chem. Chem. Phys.* **2017**, *19*, 3538–3543. [[CrossRef](#)]
28. Liu, Y.; Huang, X.; Duan, D.; Tian, F.; Liu, H.; Li, D.; Zhao, Z.; Sha, X.; Yu, H.; Zhang, H. First-Principles Study on the Structural and Electronic Properties of Metallic HfH₂ under Pressure. *Sci. Rep.* **2015**, *5*, 11381. [[CrossRef](#)]
29. Durajski, A.P. Phonon-Mediated Superconductivity in Compressed NbH₄ Compound. *Eur. Phys. J. B* **2014**, *87*, 1–6. [[CrossRef](#)]
30. Li, Y.; Hao, J.; Liu, H.; Li, Y.; Ma, Y. The Metallization and Superconductivity of Dense Hydrogen Sulfide. *J. Chem. Phys.* **2014**, *140*, 174712. [[CrossRef](#)]
31. Einaga, M.; Sakata, M.; Ishikawa, T.; Shimizu, K.; Eremets, M.I.; Drozdov, A.P.; Troyan, I.A.; Hirao, N.; Ohishi, Y. Crystal Structure of the Superconducting Phase of Sulfur Hydride. *Nat. Phys.* **2016**, *12*, 835–838. [[CrossRef](#)]
32. Ge, Y.; Zhang, F.; Yao, Y. First-Principles Demonstration of Superconductivity at 280 K in Hydrogen Sulfide with Low Phosphorus Substitution. *Phys. Rev. B* **2016**, *93*, 224513. [[CrossRef](#)]
33. Pasan, H.; Snider, E.; Munasinghe, S.; Dissanayake, S.E.; Salke, N.P.; Ahart, M.; Khalvashi-Sutter, N.; Dasenbrock-Gammon, N.; McBride, R.; Smith, G.A. Observation of Conventional near Room Temperature Superconductivity in Carbonaceous Sulfur Hydride. *arXiv* **2023**, arXiv:2302.08622.
34. Flores-Livas, J.A.; Sanna, A.; Gross, E. High Temperature Superconductivity in Sulfur and Selenium Hydrides at High Pressure. *Eur. Phys. J. B* **2016**, *89*, 1–6. [[CrossRef](#)]
35. Zhong, X.; Wang, H.; Zhang, J.; Liu, H.; Zhang, S.; Song, H.-F.; Yang, G.; Zhang, L.; Ma, Y. Tellurium Hydrides at High Pressures: High-Temperature Superconductors. *Phys. Rev. Lett.* **2016**, *116*, 057002. [[CrossRef](#)]
36. Drozdov, A.; Eremets, M.; Troyan, I. Superconductivity above 100 K in PH₃ at High Pressures. *arXiv* **2015**, arXiv:1508.06224.
37. Fu, Y.; Du, X.; Zhang, L.; Peng, F.; Zhang, M.; Pickard, C.J.; Needs, R.J.; Singh, D.J.; Zheng, W.; Ma, Y. High-Pressure Phase Stability and Superconductivity of Pnictogen Hydrides and Chemical Trends for Compressed Hydrides. *Chem. Mater.* **2016**, *28*, 1746–1755. [[CrossRef](#)]
38. Joubert, J.M.; Crivello, J.C. Stability of Erbium Hydrides Studied by DFT Calculations. *Int. J. Hydrogen Energy* **2012**, *37*, 4246–4253. [[CrossRef](#)]
39. Liu, Y.; Fan, Q.; Yang, J.; Wang, L.; Zhang, W.; Yao, G. Predicted High-Temperature Superconductivity in Rare Earth Hydride ErH₂ at Moderate Pressure. *Chin. Phys. Lett.* **2022**, *39*, 127403. [[CrossRef](#)]
40. Palasyuk, T.; Tkacz, M.; Vajda, P. High Pressure Studies of the Erbium–Hydrogen System. *Solid State Commun.* **2005**, *135*, 226–231. [[CrossRef](#)]
41. Hou, P.; Tian, F.; Li, D.; Chu, B.; Zhao, Z.; Liu, B.; Cui, T. High-Pressure Phase Transition of MH(3) (M: Er, Ho). *J. Chem. Phys.* **2014**, *141*, 054703. [[CrossRef](#)] [[PubMed](#)]
42. Kuzovnikov, M.A.; Eremets, M.I.; Drozdov, A.P.; Tkacz, M. Pressure-Induced Metallization in Erbium Trihydride. *Solid State Commun.* **2017**, *263*, 23–26. [[CrossRef](#)]
43. Wang, Y.; Lv, J.; Zhu, L.; Ma, Y. Crystal Structure Prediction Via Particle-Swarm Optimization. *Phys. Rev. B* **2010**, *82*, 094116. [[CrossRef](#)]
44. Wang, Y.; Lv, J.; Zhu, L.; Ma, Y. Calypso: A Method for Crystal Structure Prediction. *Comput. Phys. Commun.* **2012**, *183*, 2063–2070. [[CrossRef](#)]
45. Lu, C.; Chen, C. Indentation-Strain Stiffening in Tungsten Nitrides: Mechanisms and Implications. *Phys. Rev. Materials* **2020**, *4*, 043402. [[CrossRef](#)]
46. Lu, C.; Chen, C. High-Pressure Evolution of Crystal Bonding Structures and Properties of FeOOH. *J. Phys. Chem. Lett.* **2018**, *9*, 2181–2185. [[CrossRef](#)]
47. Li, X.; Xie, Y.; Sun, Y.; Huang, P.; Liu, H.; Chen, C.; Ma, Y. Chemically Tuning Stability and Superconductivity of P–H Compounds. *J. Phys. Chem. Lett.* **2020**, *11*, 935–939. [[CrossRef](#)]
48. Zhong, X.; Sun, Y.; Iitaka, T.; Xu, M.; Liu, H.; Hemley, R.J.; Chen, C.; Ma, Y. Prediction of above-Room-Temperature Superconductivity in Lanthanide/Actinide Extreme Superhydrides. *J. Am. Chem. Soc.* **2022**, *144*, 13394–13400. [[CrossRef](#)]
49. Blöchl, P.E. Projector Augmented-Wave Method. *Phys. Rev. B* **1994**, *50*, 17953. [[CrossRef](#)]
50. Kresse, G.; Furthmüller, J. Efficient Iterative Schemes for Ab Initio Total-Energy Calculations Using a Plane-Wave Basis Set. *Phys. Rev. B* **1996**, *54*, 11169. [[CrossRef](#)]
51. Perdew, J.P.; Burke, K.; Ernzerhof, M. Generalized Gradient Approximation Made Simple. *Phys. Rev. Lett.* **1996**, *77*, 3865. [[CrossRef](#)]
52. Scandolo, S.; Giannozzi, P.; Cavazzoni, C.; de Gironcoli, S.; Pasquarello, A.; Baroni, S. First-Principles Codes for Computational Crystallography in the Quantum-Espresso Package. *Z. Kristallogr.* **2005**, *220*, 574–579. [[CrossRef](#)]
53. Pickard, C.J.; Needs, R.J. Structure of Phase III of Solid Hydrogen. *Nat. Phys.* **2007**, *3*, 473–476. [[CrossRef](#)]
54. Hai, Y.-L.; Lu, N.; Tian, H.-L.; Jiang, M.-J.; Yang, W.; Li, W.-J.; Yan, X.-W.; Zhang, C.; Chen, X.-J.; Zhong, G.-H. Cage Structure and near Room-Temperature Superconductivity in TbH_N (N = 1–12). *J. Phys. Chem. C* **2021**, *125*, 3640–3649. [[CrossRef](#)]
55. Becke, A.D.; Edgecombe, K.E. A Simple Measure of Electron Localization in Atomic and Molecular Systems. *J. Chem. Phys.* **1990**, *92*, 5397–5403. [[CrossRef](#)]

56. Allen, P.B.; Dynes, R.C. Transition Temperature of Strong-Coupled Superconductors Reanalyzed. *Phys. Rev. B* **1975**, *12*, 905–922. [[CrossRef](#)]
57. Zurek, E.; Bi, T. High-Temperature Superconductivity in Alkaline and Rare Earth Polyhydrides at High Pressure: A Theoretical Perspective. *J. Chem. Phys.* **2019**, *150*, 050901. [[CrossRef](#)]

Disclaimer/Publisher’s Note: The statements, opinions and data contained in all publications are solely those of the individual author(s) and contributor(s) and not of MDPI and/or the editor(s). MDPI and/or the editor(s) disclaim responsibility for any injury to people or property resulting from any ideas, methods, instructions or products referred to in the content.